Available online at www.sciencedirect.com
ScienceDirect
Nuclear Physics B 894 (2015) 15–28
NUCLEAR PHYSICS B
www.elsevier.com/locate/nuclphysb

Entanglement entropy in a holographic p-wave superconductor model

Li-Fang Li [a], Rong-Gen Cai [b], Li Li [b], Chao Shen [a]

[a] *State Key Laboratory of Space Weather, Center for Space Science and Applied Research, Chinese Academy of Sciences, Beijing 100190, China*
[b] *State Key Laboratory of Theoretical Physics, Institute of Theoretical Physics, Chinese Academy of Sciences, Beijing 100190, China*

Received 4 January 2015; received in revised form 9 February 2015; accepted 23 February 2015

Available online 2 March 2015

Editor: Herman Verlinde

Abstract

In a recent paper, arXiv:1309.4877, a holographic p-wave model has been proposed in an Einstein–Maxwell-complex vector field theory with a negative cosmological constant. The model exhibits rich phase structure depending on the mass and the charge of the vector field. We investigate the behavior of the entanglement entropy of dual field theory in this model. When the above two model parameters change, we observe the second order, first order and zeroth order phase transitions from the behavior of the entanglement entropy at some intermediate temperatures. These imply that the entanglement entropy can indicate not only the occurrence of the phase transition, but also the order of the phase transition. The entanglement entropy is indeed a good probe to phase transition. Furthermore, the "retrograde condensation" which is a sub-dominated phase is also reflected on the entanglement entropy.

E-mail addresses: lilf@itp.ac.cn (L.-F. Li), cairg@itp.ac.cn (R.-G. Cai), liliphy@itp.ac.cn (L. Li), sc@nssc.ac.cn (C. Shen).

http://dx.doi.org/10.1016/j.nuclphysb.2015.02.023

1. Introduction

Over the past years, the AdS/CFT correspondence [1–3] has been extensively applied to the study of superconductor/superfluid in condensed matter physics. For reviews, please see Refs. [4–8]. Recently we have proposed a holographic model of p-wave superconductors in Refs. [9,10] by introducing a complex vector field ρ_μ charged under a Maxwell gauge field A_μ in the AdS bulk. This model contains two parameters, the mass and charge of the vector field. Depending on the model parameters, it has been shown that this model exhibits a rich phase structure [10,11]. In this model, the second order, first order and zeroth order phase transitions may happen. We also found the so-called "retrograde condensation", but it is sub-dominated in the sense that its free energy is much larger than the black hole solution without the vector hair. Comparing with the holographic p-wave model by introducing a SU(2) gauge field in the bulk proposed in Ref. [12], it turns out that the new p-wave model is a generalization of the one in Ref. [12] in the sense that the vector field has a general mass and gyromagnetic ratio [13].

The entanglement entropy is a good probe to quantum phase transitions and various phases in quantum field theory and many-body system. The holographic entanglement entropy proposed in Ref. [14] provides an effective way to calculate the entanglement entropy for a strongly coupled field theory (for reviews, see Refs. [15,16]). The authors of Refs. [17–21] studied the behaviors of entanglement entropy in holographic conductor/superconductor phase transition, including s-wave and p-wave cases. The results showed that the entanglement entropy decreases as one lowers temperatures, indicating the degrees of freedom are reduced at lower temperature. And the behavior of the entanglement entropy changes dramatically when the order of the phase transition changes, which implies that the entanglement entropy is indeed a good probe to phase transition. The behaviors of entanglement entropy for the holographic s-wave and p-wave superconductor/insulator model at zero temperature have also been investigated in Refs. [22–25]. This case is very similar to the study of confinement/deconfinement phase transition by the holographic entanglement entropy [26,27]. Unlike the conductor/superconductor phase transition, the entanglement entropy in the s-wave superconductor/insulator case [22–24] as a function of chemical potential is not monotonic: at the beginning of the transition, the entropy first increases and reaches its maximum at some chemical potential, and then decreases monotonically.

In this paper, we will study the entanglement entropy in this new holographic p-wave superconductor model [9,10]. The entanglement entropy is calculated for a straight strip geometry with the holographic proposal. We find that the behavior of entanglement entropy changes qualitatively in different phases as we alter the mass square m^2 and the charge q of the vector field. Our results show that the entanglement entropy can capture the characteristics of phase transitions and various phases in the holographic superconductor model. By comparing the entanglement entropy with the thermal entropy of the bulk black holes during the whole process of phase transition, we see the possibility for understanding the black hole entropy as the entanglement entropy [28–31]. Furthermore, the "retrograde condensation" which is a sub-dominated phase is also reflected on the entanglement entropy.

This paper is organized as follows. In the next section, we briefly review the holographic p-wave superconductor model. The whole system with full back reaction is solved by shooting method and the main phase structure of the model is briefly summarized. Section 3 is devoted to exploring the behaviors of the entanglement entropy in the p-wave superconductor model. We present numerical results in this section and for each given m^2, we scan a wide range of q to find all possible behaviors of the entanglement entropy. The conclusions and some discussions are included in Section 4.

2. The holographic model

Let us start with the holographic model of the p-wave superconductors proposed in Refs. [9,10]

$$S=\frac{1}{2\kappa^2}\int d^4x\sqrt{-g}\left(\mathcal{R}+\frac{6}{L^2}-\frac{1}{4}F_{\mu\nu}F^{\mu\nu}-\frac{1}{2}\rho^{\dagger}_{\mu\nu}\rho^{\mu\nu}-m^2\rho^{\dagger}_{\mu}\rho^{\mu}\right), \tag{1}$$

where $\kappa^2\equiv 8\pi G$ with G the gravitational constant, L is the radius of AdS spacetime. $F_{\mu\nu}$ and ρ_μ are Maxwell field and complex vector field, respectively, $F_{\mu\nu}=\nabla_\mu A_\nu-\nabla_\nu A_\mu$ with ∇ the covariant derivative associated with the metric $g_{\mu\nu}$, $\rho_{\mu\nu}=D_\mu\rho_\nu-D_\nu\rho_\mu$ with $D_\mu=\nabla_\mu-iqA_\mu$. And m^2 and q are the mass square and the charge of the complex vector field, respectively. Varying the action, we have the equations of motion for gauge field A_μ and charged vector field ρ_μ as

$$\begin{aligned}&\nabla^\nu F_{\nu\mu}-iq(\rho^\nu\rho^{\dagger}_{\nu\mu}-\rho^{\nu\dagger}\rho_{\nu\mu})=0,\\&D^\nu\rho_{\nu\mu}-m^2\rho_\mu=0,\end{aligned} \tag{2}$$

and the corresponding Einstein's field equations

$$\begin{aligned}\mathcal{R}_{\mu\nu}-\frac{1}{2}\mathcal{R}g_{\mu\nu}-\frac{3}{L^2}g_{\mu\nu}=&\frac{1}{2}F_{\mu\lambda}F_\nu{}^\lambda+\frac{1}{2}\mathcal{L}_m g_{\mu\nu}\\&+\frac{1}{2}\left[(\rho^{\dagger}_{\mu\lambda}\rho_\nu{}^\lambda+m^2\rho_\mu{}^{\dagger}\rho_\nu)+\mu\leftrightarrow\nu\right].\end{aligned} \tag{3}$$

The system admits an analytical solution with vanishing ρ_μ, corresponding to the normal phase, which is just the planar AdS Reissner–Nordström black hole given by [32]

$$\begin{aligned}&ds^2=-A(r)dt^2+\frac{dr^2}{A(r)}+r^2(dx^2+dy^2),\\&A(r)=r^2-\frac{1}{r}(r_h^3+\frac{\mu^2 r_h}{4})+\frac{\mu^2 r_h^2}{4r^2},\quad \phi(r)=\mu(1-\frac{r_h}{r}),\end{aligned} \tag{4}$$

with r_h is the horizon radius and μ is the chemical potential of the dual field theory. The Hawking temperature of the black hole is $T=\frac{r_h}{4\pi}(3-\frac{\mu^2}{4r_h^2})$.

When we tune the temperature, the system exhibits an instability which triggers the condensation of the charged vector field ρ_μ. Here we consider the following ansatz [10]

$$\begin{aligned}&ds^2=-f(r)e^{-\chi(r)}dt^2+\frac{dr^2}{f(r)}+r^2h(r)dx^2+r^2dy^2,\\&\rho_\nu dx^\nu=\rho_x(r)dx,\quad A_\nu dx^\nu=\phi(r)dt.\end{aligned} \tag{5}$$

The temperature T of the black hole is given by

$$T=\frac{f'(r_h)e^{-\chi(r_h)/2}}{4\pi}. \tag{6}$$

And the thermal entropy of the black hole is given by the Bekenstein–Hawking area formula: $S=2\pi V_2 r_h^2/\kappa^2$, where V_2 is the area spanned by coordinates x and y. According to the AdS/CFT correspondence, the solution (4) with vanishing ρ_ν corresponds to a conductor

(normal) phase, while the solution (5) with the complex vector hair ρ_v corresponds to the superconducting phase of the dual field theory. The process from the black hole without hair to the black hole with non-trivial vector hair mimics the conductor/superconductor phase transition. To study the behavior of the entanglement entropy during this process, we need to firstly obtain the hairy black hole solution.

With the ansatz (5), the independent equations of motion turn out to be

$$\begin{aligned}
&\phi'' + (\frac{h'}{2h} + \frac{\chi'}{2} + \frac{2}{r})\phi' - \frac{2q^2\rho_x^2}{r^2 f h}\phi = 0,\\
&\rho_x'' + (\frac{f'}{f} - \frac{h'}{2h} - \frac{\chi'}{2})\rho_x' + \frac{e^{\chi}q^2\phi^2}{f^2}\rho_x - \frac{m^2}{f}\rho_x = 0,\\
&\chi' - \frac{2f'}{f} - \frac{h'}{h} + \frac{\rho_x'^2}{rh} - \frac{re^{\chi}\phi'^2}{2f} - \frac{e^{\chi}q^2\rho_x^2\phi^2}{rf^2h} + \frac{6r}{L^2 f} - \frac{2}{r} = 0,\\
&h'' + (\frac{f'}{f} - \frac{h'}{2h} - \frac{\chi'}{2} + \frac{2}{r})h' + \frac{2\rho_x'^2}{r^2} - \frac{2e^{\chi}q^2\rho_x^2\phi^2}{r^2 f^2} + \frac{2m^2\rho_x^2}{r^2 f} = 0,\\
&(\frac{2}{r} - \frac{h'}{2h})\frac{f'}{f} + (\frac{1}{r} + \frac{\chi'}{2})\frac{h'}{h} - \frac{\rho_x'^2}{r^2 h} + \frac{e^{\chi}\phi'^2}{2f} + \frac{3e^{\chi}q^2\rho_x^2\phi^2}{r^2 f^2 h} - \frac{m^2\rho_x^2}{r^2 f h} - \frac{6}{L^2 f} + \frac{2}{r^2} = 0,
\end{aligned} \tag{7}$$

where the prime denotes the derivative with respect to r. We will use shooting method to solve the above equations (7). To do this, we have to first specify the boundary conditions for this system. Near the AdS boundary $r \to \infty$, these fields have the following expansion behaviors:

$$\begin{aligned}
&\phi = \mu - \frac{\rho}{r} + \ldots, \quad \rho_x = \frac{\rho_{x-}}{r^{\Delta_-}} + \frac{\rho_{x+}}{r^{\Delta_+}} + \ldots,\\
&f = r^2(1 + \frac{f_3}{r^3}) + \ldots, \quad h = 1 + \frac{h_3}{r^3} + \ldots, \quad \chi = 0 + \frac{\chi_3}{r^3} + \ldots,
\end{aligned} \tag{8}$$

with $\Delta_\pm = \frac{1\pm\sqrt{1+4m^2}}{2}$. According to the AdS/CFT dictionary, the constants μ and ρ can be interpreted as the chemical potential and the charge density in the dual field theory, respectively. ρ_{x-} is the source of the dual operator and ρ_{x+} gives its expectation value. To require the U(1) symmetry being broken spontaneously, we will take $\rho_{x-} = 0$ in the numerical calculation.

We impose regular conditions on the horizon $r = r_h$. Concretely, one has $f(r_h) = 0$ and $\phi(r_h) = 0$. Then we are left with five independent parameters $\{r_h, \rho_x(r_h), \phi'(r_h), h(r_h), \chi(r_h)\}$. The scaling symmetry

$$e^{\chi} \to \lambda^2 e^{\chi}, \quad t \to \lambda t, \quad \phi \to \lambda^{-1}\phi, \tag{9}$$

can be used to set $r_h = 1$ for performing numerics. Similarly, the scaling symmetries

$$\rho_x \to \lambda\rho_x, \quad x \to \lambda^{-1}x, \quad h \to \lambda^2 h, \tag{10}$$

and

$$r \to \lambda r, \quad (t, x, y) \to \lambda^{-1}(t, x, y), \quad (\phi, \rho_x) \to \lambda(\phi, \rho_x), \quad f \to \lambda^2 f, \tag{11}$$

lead us to set $\{\chi(r_h) = 0, h(r_h) = 1\}$. Thus we finally have two independent parameters $\{\rho_x(r_h), \phi'(r_h)\}$ at hand. Given $\phi'(r_h)$ as the shooting parameter to match the source free condition, i.e., $\rho_{x-} = 0$, we can solve the set of the fully coupled differential equations. The details of numerical calculation can be found in Ref. [10].

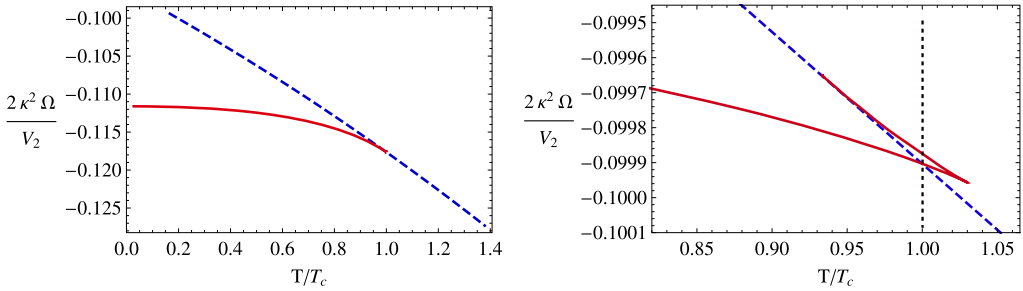

Fig. 1. The grand potential Ω as a function of temperature in the case $m^2 = 3/4$ for $q = 3/2$ (left plot) and $q = 6/5$ (right plot). The critical temperature T_c marks the occurrence of the superconducting phase. Trace the physical curve by choosing the lowest grand potential at a fixed T. The $q = 3/2$ plot shows the typical second-order phase transition. The $q = 6/5$ plot disposes a first order phase transition.

In order to determine which phase is thermodynamically favored, we should calculate the free energy of the system for both normal phase and condensed phase. We will work in grand canonical ensemble with fixed chemical potential. Following Ref. [10], the free energy Ω can be expressed as

$$\Omega = \frac{V_2}{2\kappa^2}(f_3 + h_3 - \chi_3). \tag{12}$$

For the normal phase given in (4), one has $f_3 = -r_h^3 - \frac{\mu^2 r_h}{4}$, and $h_3 = \chi_3 = 0$.

We have studied the phase structure of the model by investigating thermodynamics of various solutions of the system. There exists a critical mass square $m_c^2 = 0$. The system shows qualitatively different properties for the cases $m^2 \geq m_c^2$ and $m^2 < m_c^2$.

When $m^2 \geq m_c^2$, there exists a critical charge q_c, which depends on the value of m^2. If $q \geq q_c$, the system undergoes a second order phase transition at the critical temperature $T = T_c$ from the conductor (normal) phase for temperature $T > T_c$ to the superconducting phase for temperature $T < T_c$. On the other hand, if $q < q_c$, the phase transition becomes a first order one, which can be seen from Fig. 1.

When $m^2 < m_c^2$, the range of charge q is divided into three regimes by two critical charges, q_α and q_β, which also depends on the value of m^2. If $q \geq q_\alpha$, the system is in a normal phase when $T > T_{2c}$, in a superconducting phase when $T_{0c} < T < T_{2c}$, and in the normal phase when $T < T_{0c}$. There exist a second order phase transition at $T = T_{2c}$, where the free energy is continuous, and a zeroth order phase transition at $T = T_{0c}$, where the free energy is discontinuous. If $q_\beta < q < q_\alpha$, the second order phase transition is replaced by a first order one at $T = T_{1c}$. If $q \leq q_\beta$, the black hole solution with vector hair can exist, but its free energy is always larger than the one without the vector hair. The condensation is called "retrograde condensation". The solution is sub-dominated and therefore this phase will not appear in the phase diagram. In this case, the system is always in the normal phase. We can see these clearly from Fig. 2. Note that all the critical temperatures T_c, T_{2c}, T_{1c} and T_{0c} depend on the model parameters m^2 and q.

In summary, depending on the model parameters m^2 and q, the model exhibits a rich phase structure. The details are summarized in Table 1. In the spirit of AdS/CFT correspondence, the mass square m^2 of the vector field is related to the conformal dimension of the dual vector operator, while the charge q of the vector field corresponds to the "charge" of the condensate. From the bulk point of view the charge q is the coupling parameter between the vector field and the bulk Maxwell field and governs the back reaction strength of the matter fields on the

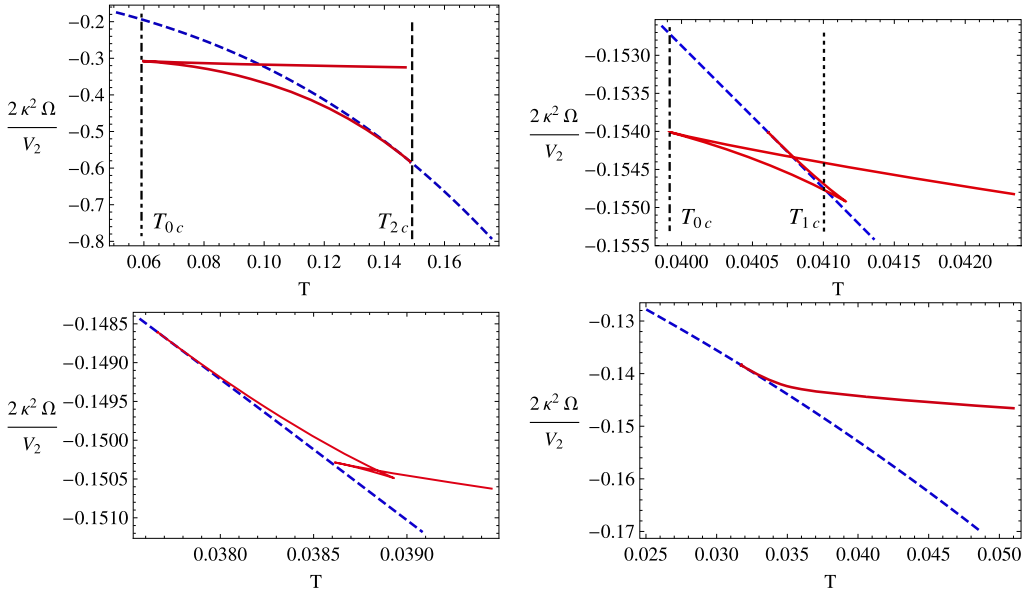

Fig. 2. The free energy Ω as a function of temperature with vector condensation (solid red), and without the vector condensation (dashed blue) in the cases $m^2 = -3/16$ and $q = 2$ (top left), $q = 39/40$ (top right), $q = 19/20$ (bottom left), $q = 9/10$ (bottom right). The $q = 2$ plot shows the second order phase transition but the condensed phase terminates at finite low temperature T_0. The $q = 39/40$ plot exhibits a first order phase transition but also the superconducting phase terminates at finite low temperature T_0. The $q = 19/20$ and $q = 9/10$ plots demonstrate that the condensed phase has free energy much larger than the normal phase and thus is not thermodynamical favored. (For interpretation of the references to color in this figure, the reader is referred to the web version of this article.)

Table 1
The phase transition and its order with respect to the charge q and the mass square m^2. Here N stands for conductor (normal) phase with RN–AdS black hole solution, while SC for the superconducting phase with black hole solutions with vector hair. 0th, 1st, and 2nd stand for the zeroth order, first order and second order phase transition, respectively. $m_c^2 = 0$. q_c, q_α, q_β are some critical values depending on m^2. T_c, T_{0c}, T_{1c}, and T_{2c} are some critical temperatures depending on m^2 and q.

Charge					
	Phase transition and its order for $m^2 \geq m_c^2$				
$q \geq q_c$	$T > T_c$, N		$T = T_c$, 2nd	$T < T_c$, SC	
$q < q_c$	$T > T_c$, N		$T = T_c$, 1st	$T < T_c$, SC	
	Phase transition and its order for $m^2 < m_c^2$				
$q \geq q_\alpha$	$T > T_{2c}$, N	$T = T_{2c}$, 2nd	$T_{0c} < T < T_{2c}$, SC	$T = T_{0c}$, 0th	$T < T_{0c}$, N
$q_\beta < q < q_\alpha$	$T > T_{1c}$, N	$T = T_{1c}$, 1st	$T_{0c} < T < T_{1c}$, SC	$T = T_{0c}$, 0th	$T < T_{0c}$, N
$q \leq q_\beta$	N				

background geometry. In this sense the charge q plays the same role as the coupling parameter $\hat{g}^2$ in the Einstein–Yang–Mills theory [33]. Thus one may think that the parameter q counts the additional degrees of freedom in the dual CFT [33]. In this way the mass square and charge of the vector filed control the phase structure of the dual CFT.

In addition, let us mention here that the zeroth order phase transition with discontinuous free energy looks strange at first glance, but it has been argued that it could appear in superconduc-

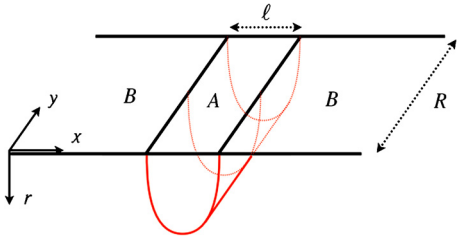

Fig. 3. The minimal surface γ_A corresponding to the strip region $\mathcal{A}$ in the boundary. The quantity ℓ sets the size of region $\mathcal{A}$.

tivity and superfluid [34]. In that reference an exact solvable model has also been proposed. Furthermore, the zeroth order phase transition also appears in the extended phase space of AdS black hole thermodynamics [35,36]. But we remind here that the zeroth order phase transition might not be physical in this holographic superconductor model. The reason is that in this model we have only considered two phases, the normal phase described by the RN–AdS black hole and the superconducting phase described by black hole with vector hair, both solutions are of the translation symmetry in the transversal directions. If further consider other components of the complex vector field and/or the case without the transversal translation symmetry, we might find other phases which have a lower free energy so that those phases are more stable and the zeroth order phase transition discussed in the above will be replaced by a first order or second order phase transition. But in the present paper we limit ourselves to the case summarized in Table 1.

3. Entanglement entropy

In the framework of AdS/CFT correspondence, a holographic method to calculate the entanglement entropy has been proposed in Ref. [14]. Following Ref. [14], for a conformal field theory (CFT) which has a dual gravitational configuration living in one higher dimension, the entanglement entropy of the CFT in a subsystem $\mathcal{A}$ with its complement can be obtained by searching the minimal area surface $\gamma_{\mathcal{A}}$ extended into the bulk with the same boundary $\partial\mathcal{A}$ of $\mathcal{A}$. That is, the entanglement entropy of $\mathcal{A}$ with its complement is given by the "area law"

$$S_{\mathcal{A}} = \frac{2\pi}{\kappa^2} Area(\gamma_{\mathcal{A}}). \tag{13}$$

In this section we will study the behavior of entanglement entropy in this holographic p-wave superconductor model. We will consider a belt geometry with a finite width l along the x direction and extends in y direction. The holographic dual surface γ_A is defined as a two-dimensional surface

$$t = 0, \quad r = r(x), \quad -\frac{R}{2} < y < \frac{R}{2} \ (R \to \infty). \tag{14}$$

R is the regularized length in y direction. To avoid the UV divergence, we consider the subsystem $\mathcal{A}$ sits on the slice $r = \frac{1}{\epsilon}$ with $\epsilon \to 0$ the UV cutoff. More specifically, the holographic surface γ_A starts from $x = \frac{\ell}{2}$ at $r = \frac{1}{\epsilon}$, extends into the bulk until it reaches $r = r_*$, then returns back to the AdS boundary $r = \frac{1}{\epsilon}$ at $x = -\frac{\ell}{2}$. The smooth configuration is shown in Fig. 3.

Note that there might also exist a piece-wise configuration for which the dual surface goes straight down from the boundary to the horizon, see, e.g., Fig. 1 in Ref. [37]. However, it has been suggested that generically the smooth one would always dominate at finite temperature

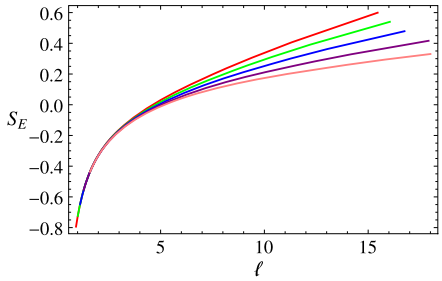

Fig. 4. The entanglement entropy as a function of belt width at fixed temperature in the case of $m^2 = 3/4$ and $q = 3/2$. The curves from top to bottom correspond to $T \approx 0.0179, 0.0173, 0.0165, 0.0152, 0.0132$, respectively.

involving black hole horizons [37]. So following the previous studies [17–19], we only consider the case with smooth configuration.

The entanglement entropy of such a subsystem is given by

$$S_{\mathcal{A}} = \frac{4\pi L}{\kappa^2} R \int_{r_*}^{\frac{1}{\epsilon}} \frac{r^3}{\sqrt{(r^4 - \frac{h(r_*)}{h(r)} r_*^4) f(r)}} dr = \frac{4\pi L}{\kappa^2} R (\frac{1}{\epsilon} + S_E), \tag{15}$$

where the UV divergence part $1/\epsilon$ has been separated from the total entropy. Thus S_E is the finite part of physical relevance. The width l of the subsystem $\mathcal{A}$ and r_* are connected by the relation

$$\frac{l}{2} = \int_{r_*}^{\frac{1}{\epsilon}} \frac{dx}{dr} dr = \int_{r_*}^{\frac{1}{\epsilon}} \frac{1}{\sqrt{\left(\frac{r^6 h^2(r)}{r_*^4 h(r_*)} - r^2 h(r)\right) f(r)}} dr. \tag{16}$$

We are here interested in the finite part S_E for the entanglement entropy, which is of physical relevance. With the background solutions $h(r)$ and $f(r)$ by solving the equations of motion for the model, we can calculate the entanglement entropy numerically.

Our results show that the entanglement entropy S_E with respect to strip width l behaves quite similar for different parameters m^2 and q. The entanglement entropy versus strip width l is shown in Fig. 4 with $m^2 = 3/4$ and $q = 3/2$. In this case, the critical temperature is $T_c \approx 0.0179$ [10]. Different colorful curves reveal how the entanglement entropy changes with respect to the belt width for different temperatures. Note that in the present paper we are working in the grand canonical ensemble with fixed chemical potential $\mu = 1$. From the top to bottom, the temperature decreases. The curve at the top is for the case with the critical temperature T_c, which is identical with the case of the normal phase. From Fig. 4, we can see that the slope of the curves decreases when the temperature lowers in the superconducting phase. This is expected because the lower the temperature is, the more the degrees of freedom are condensed.

For a fixed temperature, say $T \approx 0.0165$, the blue curve describes a monotonically increasing behavior of the entanglement entropy with respect to the belt width. The entanglement entropy is dominated by the connected surface γ_A. The wider belt width corresponds to a larger area of the holographic surface. This dependence of the entanglement entropy on l is non-trivial. More explicitly, for large l, we see that S_E changes linearly with l. This is because in large l limit, the main contribution of the integration in (15) and (16) to S_E comes from the region near $r = r_* \sim r_h$. Near the horizon, we can deduce the linear relation $S_E \sim l$. In contrast, the value of S_E seems to be power-law divergent as l goes to zero.

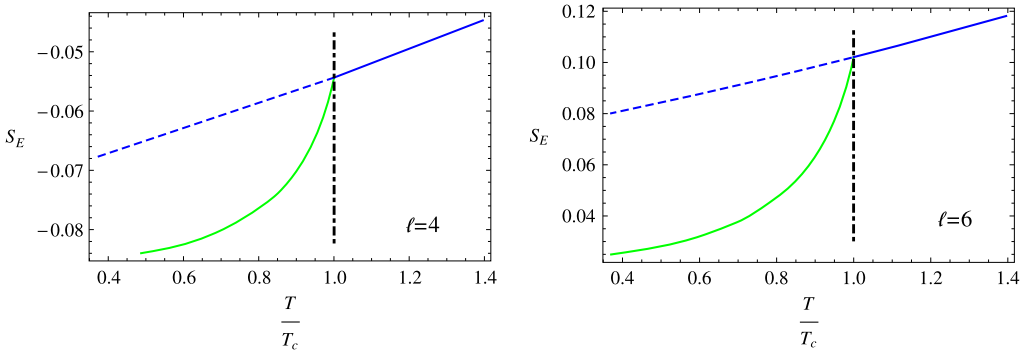

Fig. 5. The entanglement entropy as a function of temperature with fixed belt width in the case $m^2 = 3/4$ and $q = 3/2$ (left plot for $\ell = 4$ and right plot for $\ell = 6$). The blue curves correspond to the entanglement entropy in the normal phase, while the green curves are for the superconducting phase. The physical curve is determined by tracing the lower entropy at a given T. The critical temperature is $T_c \approx 0.00342\mu$. (For interpretation of the references to color in this figure, the reader is referred to the web version of this article.)

As shown in Table 1, the phase structure is quite different for the $m^2 \geq m_c^2$ case and $m^2 < m_c^2$ case. In the following we will explore the behavior of the entanglement entropy quantitatively for these two cases, respectively.

3.1. The case with $m^2 \geqslant m_c^2$

In this case we take $m^2 = 3/4$ as a typical example. For other values of the mass, the behavior of entanglement entropy is the same qualitatively. Note that in this case, the critical charge $q_c \approx 1.3575$ [10].

Fig. 5 shows that the entanglement entropy is continuous at critical temperature T_c, but its slope is not. This discontinuity signals a significant reorganization of the degrees of freedom of the system. Since there is a condensate generated at the transition point, it is expected that there is a reduction of degrees of freedom. The behavior of the entanglement entropy versus temperature indicates a typical second order phase transition.

As we decrease q to $q = 6/5$ which is less than $q_c \approx 1.3575$, the entanglement entropy as a function of temperature is presented in Fig. 6. In such a case, the entanglement entropy has a jump from the normal phase to the superconducting phase at the critical temperature, showing the behavior of a first order phase transition, which is also consistent with the behavior of the thermal entropy. This example shows that entanglement entropy indeed can tell us the appearance of phase transition and its order.

From Figs. 5 and 6, we can also see that the behavior of entanglement entropy is the same qualitatively for the belt widths $l = 4$ and $l = 6$. The only difference is that the value of the entanglement entropy for larger l is larger at the same temperature T. This is consistent with the observation in Fig. 4.

Note that the behavior of the entanglement entropy observed here is qualitatively the same as the one of the thermal entropy considered in the paper [10]. Considering the thermal entropy is equivalent to the black hole entropy in the holographic setup, our results indicate that the black hole entropy could be due to the entanglement entropy [28–31].

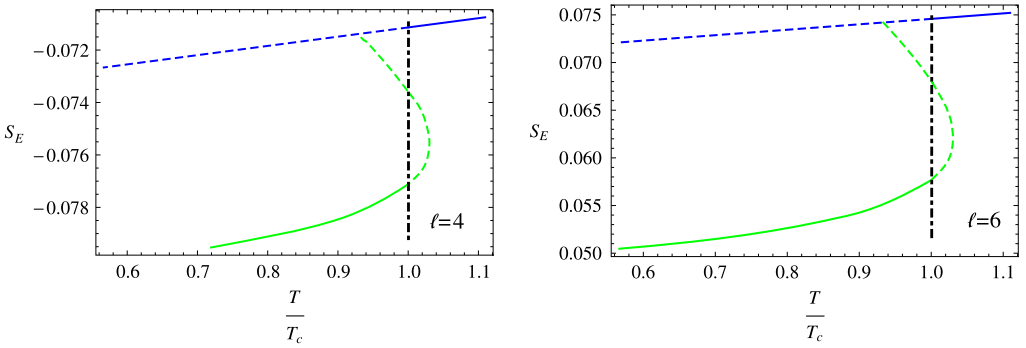

Fig. 6. The entanglement entropy as a function of temperature with fixed belt width in the case $m^2 = 3/4$ and $q = 6/5$ (left plot for $\ell = 4$ and right plot for $\ell = 6$). The blue curves are from the AdS Reissner–Nordström solutions, while the green curves are from superconductor solutions. The physical curve is selected by choosing the solid blue curve above the critical temperature $T_c \approx 0.00342\mu$, denoted by the vertical dash-dotted line, and the curve which has the lowest entropy below T_c. (For interpretation of the references to color in this figure, the reader is referred to the web version of this article.)

3.2. *The case with $m^2 < m_c^2$*

In this case we take $m^2 = -3/16$ as a typical example (the BF bound is still satisfied in this case). Note that in this case the critical charges are $q_\alpha \approx 1.0175$ and $q_\beta \approx 0.9537$ [10], respectively. We find different behaviors of entanglement entropy for the cases $q \geq q_\alpha$, $q_\alpha > q > q_\beta$, and $q \leq q_\beta$, respectively. In Figs. 7–10 we plot the entanglement entropy versus temperature for the cases of $q = 2$, $q = 39/40$, $q = 19/20$ and $q = 9/10$, respectively.

In Fig. 7 we plot the entanglement entropy versus temperature for $q = 2$ as an example in the case of $q > q_\alpha$. We can see that at the second order transition point $T = T_{2c}$, the entanglement entropy is continuous, but its slope is not, while at the zeroth order transition point $T = T_{0c}$, the entanglement entropy has a jump. In addition, in the superconducting phase, the entanglement entropy has two branches: the solid green curve is physically favored, while the dashed one is not physically favored since for the latter, the solution has a higher free energy than the hairy black hole solution for the former.

For the case $q_\beta < q < q_\alpha$, we consider the example with $q = 39/40$. The behavior of the entanglement entropy as a function of temperature is shown in Fig. 8. We can see from the figure that the entanglement entropy has a jump both at the first order transition point at $T = T_{1c}$ and at the zeroth order transition point at $T = T_{0c}$. But the two situations are different. For the former, both the entanglement entropies in the normal phase and superconducting phase can be connected by a metastable superconducting phase (dashed curve), while for the latter, there does not exist such a metastable phase.

For the case $q \leq q_\beta$, we consider two examples of $q = 19/20$ and $q = 9/10$. Their behaviors of entanglement entropy are shown in Figs. 9 and 10, respectively. In this case, the condensation appears in the high temperature regime, and hairy black hole solutions have higher free energy than the RN–AdS black hole at the same temperature, therefore the hairy black hole solutions are not physically favored (bottom left and bottom right plots in Fig. 2). We see from the figure that the entanglement entropy S_E is multi-valued for $q = 19/20$, while it monotonically decreases when the temperature increases for $q = 9/10$, for the hairy black hole solutions.

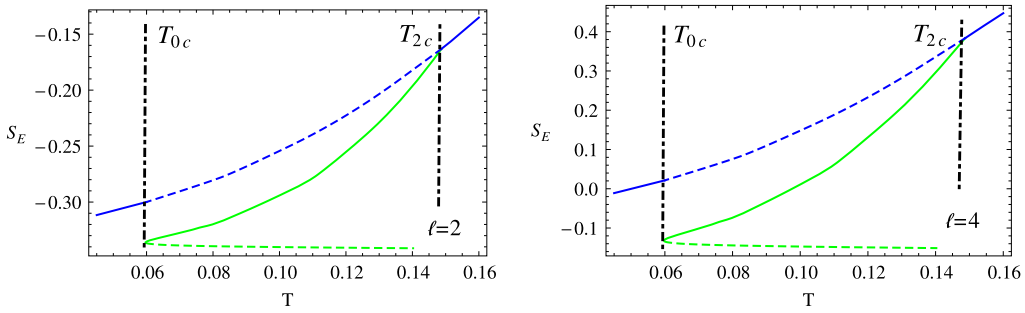

Fig. 7. The entanglement entropy with respect to temperature with fixed belt width in the case $m^2 = -3/16$ and $q = 2$ (left plot for $\ell = 2$ and right plot for $\ell = 4$). The blue curves are from the AdS Reissner–Nordström solutions, while the green curves are from superconducting solutions. The physical branch is selected by choosing the solid curve, which shows a 0th order phase transition at T_{0c} and a 2nd phase transition at T_{2c}. (For interpretation of the references to color in this figure, the reader is referred to the web version of this article.)

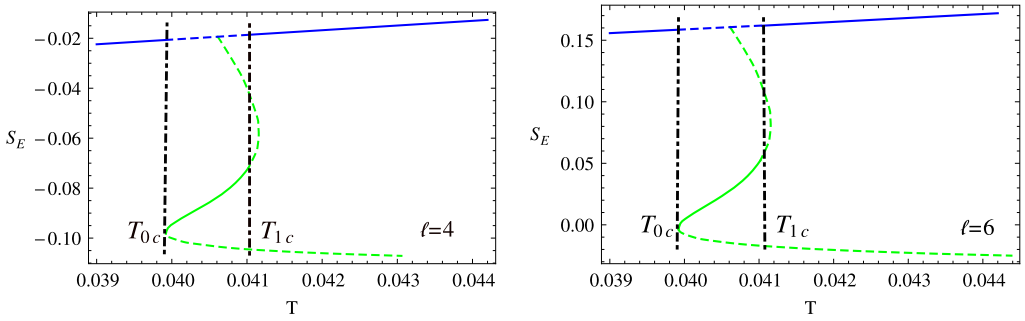

Fig. 8. The entanglement entropy with respect to temperature with fixed belt width in the case $m^2 = -3/16$ and $q = 39/40$ (left plot for $\ell = 4$ and right plot for $\ell = 6$). The blue curves are from the AdS Reissner–Nordström solutions, while the green curves are from superconductor solutions. The physical branch is selected by choosing the solid curve, which shows a 0th order phase transition at T_{0c} and 1st order phase transition at T_{1c}. (For interpretation of the references to color in this figure, the reader is referred to the web version of this article.)

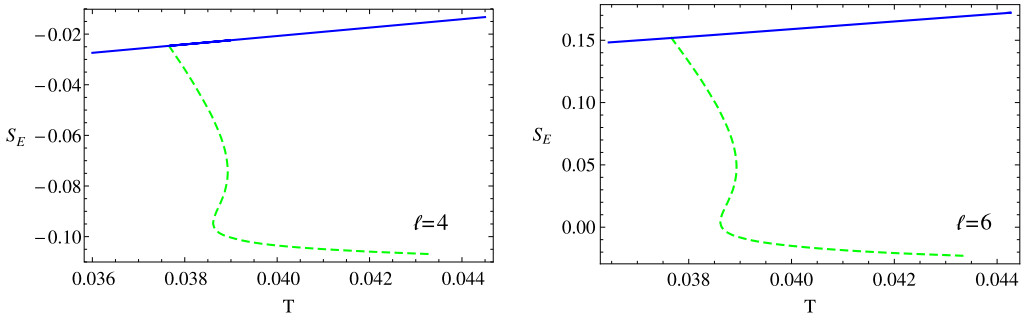

Fig. 9. The entanglement entropy as a function of temperature at fixed belt width in $m^2 = -3/16$, $q = 19/20$ case (left plot for $\ell = 4$ and right plot for $\ell = 6$). The solid curves are from the AdS Reissner–Nordström solutions, while the dashed curves are the "retrograde condensation" phases. There is no phase transition at all in such case.

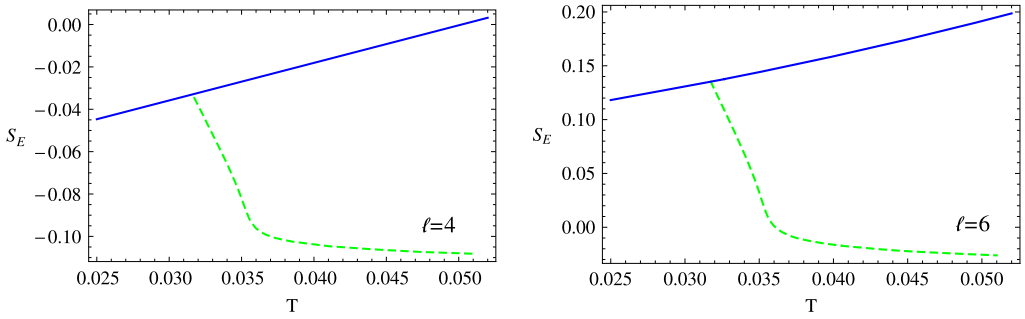

Fig. 10. The entanglement entropy as a function of temperature at fixed belt width in $m^2 = -3/16$, $q = 9/10$ case (left plot for $\ell = 4$ and right plot for $\ell = 6$). The solid curves are from the AdS Reissner–Nordström solutions, while the dashed curves are from the "retrograde condensation" phases. There is no phase transition at all in such case.

Once again, we find that the behaviors of the entanglement entropy are the same qualitatively for different belt widths. Comparing the behaviors of the entanglement entropy with corresponding ones of thermal entropy studied in [10], we find that both the behaviors are the same qualitatively. This further supports that entanglement entropy is a good measure of degrees of freedom for quantum field theory, and also it tells that entanglement entropy is a good probe to phase transition and various phases in holographic superconductor models.

4. Conclusions and discussions

In recent works [9–11] we have constructed a holographic p-wave superconductor model in a four-dimensional Einstein–Maxwell-complex vector field theory with a negative cosmological constant. Depending on the mass square m^2 and the charge q of the complex vector field ρ_μ, the model exhibits a rich phase structure. The second order, first order and even zeroth order phase transitions would appear in this model and the so-called "retrograde condensation" also could happen in some parameter space. In this paper we have continued to study this model by investigating the behavior of holographic entanglement entropy for a belt geometry at the AdS boundary.

The main results of this paper can be found from Figs. 4 to 10. In Fig. 4 we show the behavior of the entanglement entropy with respect to the belt width for different temperatures in the superconducting phase. For the case with a fixed temperature, the entanglement entropy increases with the belt width, while in the case for a fixed width, it decreases when the temperature is lowered. This is expected because entanglement entropy is a measure of degrees of freedom for the dual field theory and when the temperature lowers, more degrees of freedom will be condensed.

Figs. 5–6 and 7–10 show the behavior of the entanglement entropy with respect to temperature in various phases, which depend on the model parameters m^2 and q. We have observed that at the second order phase transition point, the entanglement entropy is continuous, but its slop is discontinuous, while at the first order and the zeroth order transition points, the entanglement entropy has a jump. But for the latter two cases, the situations are different. For the first order phase transition, the two entanglement entropies for the normal phase and the superconducting phase can be connected by a metastable condensed phase, while in the case of the zeroth order phase transition, there does not exist the metastable condensed phase. Here we remind again that the zeroth order phase transition discussed in this paper might be not physical, as we mentioned in the above, because there might exist more stable non-trivial black hole solutions in this model.

In this present study, we have seen that the behavior of entanglement entropy always shares some similarity with thermal entropy [10]. The similarity can be understood as the fact that the entanglement entropy is contaminated by the thermal fluctuation at finite temperature, and the entanglement entropy approaches to the thermal entropy at high temperatures. In this sense, the entanglement entropy is a unique order parameter one can use even at zero temperature and it deserves to further investigate the behavior in the holographic superconductor/insulator transition in the Einstein–Maxwell-complex vector model. Indeed, the entanglement entropy in some superconductor/insulator models at zero temperature were studied and some interesting behaviors were uncovered [22–24].

Note that in this paper we have only studied the entanglement entropy with finite width along the x direction. In such a model, the spatial rotational symmetry is broken in the superconducting phase. To capture the anisotropy in x direction and y direction, ones should also study the entanglement entropy along y direction. We do not calculate it here because the behavior of the entanglement entropy along y direction is expected to be qualitatively similar to the case in x direction. As a non-local quantity, the entanglement entropy describes the new degrees of freedom emerging in the superconducting phase. Since the degree of anisotropy of the superconducting phase is characterized by the value of condensate, therefore, it is not expected to have qualitative difference for entanglement entropy between along x direction and y direction [25].

Furthermore, apart from the entanglement entropy, there is another nonlocal quantity, Wilson loop, which can describe some aspects of gauge field theory. The study of such a quantity can also shed some lights into the holographic superconducting phase transition. We expect to report further progress on these issues in future.

Acknowledgements

This work was supported in part by the National Natural Science Foundation of China (No. 11035008, No. 11375247, No. 11205226 and No. 41231066), and in part by the Ministry of Science and Technology of the People's Republic of China under Grant No. 2010CB833004. L.F.L. and C.S. would like to appreciate the National Basic Research Program of China (973 Program) Grant No. 2011CB811404 and the Specialized Research Fund for State Key Laboratories.

References

[1] J.M. Maldacena, The large N limit of superconformal field theories and supergravity, Adv. Theor. Math. Phys. 2 (1998) 231, Int. J. Theor. Phys. 38 (1999) 1113, arXiv:hep-th/9711200.
[2] S.S. Gubser, I.R. Klebanov, A.M. Polyakov, Gauge theory correlators from non-critical string theory, Phys. Lett. B 428 (1998) 105, arXiv:hep-th/9802109.
[3] E. Witten, Anti-de Sitter space and holography, Adv. Theor. Math. Phys. 2 (1998) 253, arXiv:hep-th/9802150.
[4] S.A. Hartnoll, Lectures on holographic methods for condensed matter physics, Class. Quantum Gravity 26 (2009) 224002, arXiv:0903.3246 [hep-th].
[5] C.P. Herzog, Lectures on holographic superfluidity and superconductivity, J. Phys. A 42 (2009) 343001, arXiv:0904.1975 [hep-th].
[6] J. McGreevy, Holographic duality with a view toward many-body physics, Adv. High Energy Phys. 2010 (2010) 723105, arXiv:0909.0518 [hep-th].
[7] G.T. Horowitz, Introduction to holographic superconductors, Lect. Notes Phys. 828 (2011) 313, arXiv:1002.1722 [hep-th].
[8] R.G. Cai, L. Li, L.F. Li, R.Q. Yang, Introduction to holographic superconductor models, arXiv:1502.00437 [hep-th].
[9] R.G. Cai, S. He, L. Li, L.F. Li, A holographic study on vector condensate induced by a magnetic field, J. High Energy Phys. 1312 (2013) 036, arXiv:1309.2098 [hep-th].

[10] R.G. Cai, L. Li, L.F. Li, A holographic P-wave superconductor model, J. High Energy Phys. 1401 (2014) 032, arXiv:1309.4877 [hep-th].
[11] R.-G. Cai, L. Li, L.-F. Li, R.-Q. Yang, Towards complete phase diagrams of a holographic p-wave superconductor model, J. High Energy Phys. 1404 (2014) 016, arXiv:1401.3974 [gr-qc].
[12] S.S. Gubser, S.S. Pufu, The gravity dual of a p-wave superconductor, J. High Energy Phys. 0811 (2008) 033, arXiv:0805.2960 [hep-th].
[13] R.-G. Cai, L. Li, L.-F. Li, Y. Wu, Vector condensate and AdS soliton instability induced by a magnetic field, J. High Energy Phys. 1401 (2014) 045, arXiv:1311.7578 [hep-th].
[14] S. Ryu, T. Takayanagi, Holographic derivation of entanglement entropy from AdS/CFT, Phys. Rev. Lett. 96 (2006) 181602, arXiv:hep-th/0603001.
[15] T. Nishioka, S. Ryu, T. Takayanagi, Holographic entanglement entropy: an overview, J. Phys. A 42 (2009) 504008, arXiv:0905.0932 [hep-th].
[16] T. Takayanagi, Entanglement entropy from a holographic viewpoint, arXiv:1204.2450 [gr-qc].
[17] T. Albash, C.V. Johnson, Holographic studies of entanglement entropy in superconductors, J. High Energy Phys. 1205 (2012) 079, arXiv:1202.2605 [hep-th].
[18] R.-G. Cai, S. He, L. Li, Y.-L. Zhang, Holographic entanglement entropy on p-wave superconductor phase transition, J. High Energy Phys. 1207 (2012) 027, arXiv:1204.5962 [hep-th].
[19] R.E. Arias, I.S. Landea, Backreacting p-wave superconductors, J. High Energy Phys. 1301 (2013) 157, arXiv:1210.6823 [hep-th].
[20] Y. Peng, Q. Pan, Holographic entanglement entropy in general holographic superconductor models, J. High Energy Phys. 1406 (2014) 011, arXiv:1404.1659 [hep-th].
[21] W. Yao, J. Jing, Holographic entanglement entropy in metal/superconductor phase transition with Born–Infeld electrodynamics, Nucl. Phys. B 889 (2014) 109, arXiv:1408.1171 [hep-th].
[22] R.-G. Cai, S. He, L. Li, Y.-L. Zhang, Holographic entanglement entropy in insulator/superconductor transition, J. High Energy Phys. 1207 (2012) 088, arXiv:1203.6620 [hep-th].
[23] R.-G. Cai, S. He, L. Li, L.-F. Li, Entanglement entropy and Wilson loop in Stückelberg holographic insulator/superconductor model, J. High Energy Phys. 1210 (2012) 107, arXiv:1209.1019 [hep-th].
[24] W. Yao, J. Jing, Holographic entanglement entropy in insulator/superconductor transition with Born–Infeld electrodynamics, J. High Energy Phys. 1405 (2014) 058, arXiv:1401.6505 [hep-th].
[25] R.-G. Cai, L. Li, L.-F. Li, R.-K. Su, Entanglement entropy in holographic p-wave superconductor/insulator model, J. High Energy Phys. 1306 (2013) 063, arXiv:1303.4828 [hep-th].
[26] T. Nishioka, T. Takayanagi, AdS bubbles, entropy and closed string tachyons, J. High Energy Phys. 0701 (2007) 090, arXiv:hep-th/0611035.
[27] I.R. Klebanov, D. Kutasov, A. Murugan, Entanglement as a probe of confinement, Nucl. Phys. B 796 (2008) 274, arXiv:0709.2140 [hep-th].
[28] T. Jacobson, Black hole entropy and induced gravity, arXiv:gr-qc/9404039.
[29] D.N. Kabat, Black hole entropy and entropy of entanglement, Nucl. Phys. B 453 (1995) 281, arXiv:hep-th/9503016.
[30] S.N. Solodukhin, Entanglement entropy of black holes and AdS/CFT correspondence, Phys. Rev. Lett. 97 (2006) 201601, arXiv:hep-th/0606205.
[31] R. Emparan, Black hole entropy as entanglement entropy: a holographic derivation, J. High Energy Phys. 0606 (2006) 012, arXiv:hep-th/0603081.
[32] R.G. Cai, Y.Z. Zhang, Black plane solutions in four-dimensional space–times, Phys. Rev. D 54 (1996) 4891, arXiv:gr-qc/9609065.
[33] M. Ammon, J. Erdmenger, V. Grass, P. Kerner, A. O'Bannon, On holographic p-wave superfluids with backreaction, Phys. Lett. B 686 (2010) 192, arXiv:0912.3515 [hep-th].
[34] V.-P. Maslov, Zeroth-order phase transitions, Math. Notes - Ross. Akad. 76 (2004) 697.
[35] N. Altamirano, D. Kubiznak, R.B. Mann, Reentrant phase transitions in rotating AdS black holes, Phys. Rev. D 88 (2013) 101502, arXiv:1306.5756 [hep-th].
[36] S. Gunasekaran, R.B. Mann, D. Kubiznak, Extended phase space thermodynamics for charged and rotating black holes and Born–Infeld vacuum polarization, J. High Energy Phys. 1211 (2012) 110, arXiv:1208.6251 [hep-th].
[37] I. Bah, A. Faraggi, L.A. Pando Zayas, C.A. Terrero-Escalante, Holographic entanglement entropy and phase transitions at finite temperature, Int. J. Mod. Phys. A 24 (2009) 2703, arXiv:0710.5483 [hep-th].